Effect of thermal annealing on the hyperfine interaction in InAs/GaAs quantum dots

M. Yu. Petrov,[1,*] I. V. Ignatiev,[1] S. V. Poltavtsev,[1] A. Greilich,[2] A. Bauschulte,[2] D. R. Yakovlev,[2,3] and M. Bayer[2]
[1]*Faculty of Physics, St. Petersburg State University, St. Petersburg 198504, Russia*
[2]*Experimentelle Physik II, Technische Universität Dortmund, Dortmund D-44227, Germany*
[3]*A. F. Ioffe Physico-Technical Institute, Russian Academy of Sciences, St. Petersburg 194021, Russia*
(Received 13 November 2007; revised manuscript received 11 April 2008; published 18 July 2008)

The hyperfine interaction of an electron with the unpolarized nuclei in thermally annealed self-assembled InAs/GaAs quantum dots (QDs) is theoretically analyzed. For this purpose, the thermal annealing process of the quantum dots is numerically modeled to obtain the nuclear composition as well as the electron ground state in the QDs. To check the reliability of calculations, the ground-state excitonic transition energies are compared with photoluminescence data from a set of annealed dots. From these results, the electron localization volume and the partial contributions of the In, Ga, and As nuclei to the hyperfine interaction are calculated as functions of annealing temperature. The contribution of the indium nuclei to the hyperfine interaction dominates up to high temperatures of the annealing (T_a=980 °C), for which the In content in the dots does not exceed 25%. Simulations of the effect of the nuclear-spin fluctuations on the electron-spin polarization decay are in good agreement with the experiment.

DOI: 10.1103/PhysRevB.78.045315 PACS number(s): 72.25.Rb, 78.67.Hc, 78.55.Cr, 73.22.Dj

I. INTRODUCTION

The hyperfine interaction of an electron with a nuclear-spin ensemble is the most effective mechanism for electron-spin relaxation in quantum dots (QDs) (Refs. 1–3). Due to the limited number of QD nuclei interacting with the electron spin, the coaction of the randomly oriented nuclear spins leads to a nonzero total spin of the nuclear system.[4,5] This total spin acts on the electron spin as an effective magnetic field B_N, with random magnitude and orientation. The electron spin rapidly precesses about this fluctuating field, resulting in a decay of the electron-spin polarization in a QD ensemble. Typical spin decay times are about a fraction of a nanosecond for InAs/GaAs QDs (Ref. 2). At the same time, the electron-spin relaxation due to other processes, such as electron-phonon interaction, is a few orders of magnitude slower.[6,7]

The hyperfine interaction strength depends on the number of nuclei covered by the electron wave function and, therefore, on the electron localization volume.[4] Scaling the QD effective size, one may therefore control the hyperfine interaction. A way to increase the QD size is postgrowth thermal annealing of a QD heterostructure at relatively high temperatures. However, the annealing also changes the nuclear composition of the dots since it causes diffusion of indium from the QDs into the barriers and of gallium in reverse direction, which results in a decrease in the confinement potential and an enlargement of the size.[8–10]

In this paper, we theoretically analyze the effect of postgrowth thermal annealing on the electron-nuclei hyperfine interaction in self-assembled InAs/GaAs QDs. We present a numerical model which allows us to simulate the process of annealing, in order to calculate the In and Ga atom distribution profiles over the heterostructure as well as the ground-state electron wave function in the dots. The calculations are adapted to realistic parameters by comparison with experimental data on the ground-state interband transitions in the corresponding QD samples.[3,11,12] This allows us to model the hyperfine interaction of an electron with the nuclei as a function of annealing temperature parameter free and makes it possible to quantitatively describe the electron-spin depolarization via the hyperfine interaction with nuclei and the suppression of this effect by a longitudinal magnetic field.

II. QUANTUM DOT MODEL

Typically self-assembled InAs/GaAs QDs have truncated pyramid or lens shapes with base diameters d=15–30 nm and heights h=5–15 nm (Ref. 13). The size of the QDs depends on the growth parameters, in particular on the nominal thickness of the deposited indium layer. In addition, there is a spread of dot sizes within a QD ensemble. To be specific, we consider the heterostructure investigated in Refs. 3, 11, and 12. A cross-section image of the as-grown sample obtained by scanning electron microscopy (SEM) is shown in Fig. 1. Though the spatial resolution is not high, we estimate the base diameter of the QDs to be about 20–30 nm. A higher spatial resolution as obtainable by transmission electron microscopy is not available for this heterostructure.

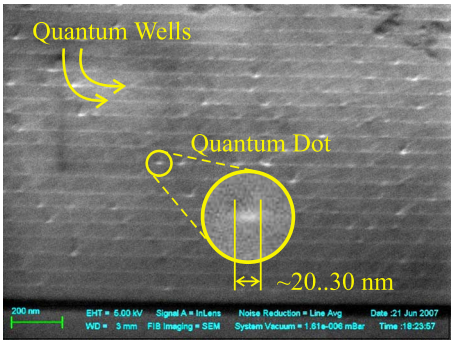

FIG. 1. (Color online) Scanning electron microscopy image of the cross section of the heterostructure with as-grown InAs/GaAs QDs.

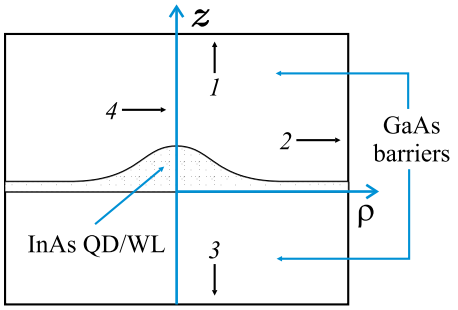

FIG. 2. (Color online) Sketch of the QD model. Cross section of the heterostructure and the computational region (see text for details).

Therefore, we extract the parameters of the QD geometry by analyzing photoluminescence (PL) spectra with respect to the dependence of the carrier quantization energies and optical transitions on these parameters (see below). We ignore the statistical spread of the QD sizes within an ensemble. For simplicity we consider cylindrically symmetric QDs with a smooth bell-like shape. A sketch of the QD model is given in Fig. 2. Using cylindrical coordinates, we define the z axis by the growth direction (symmetry axis) and ρ is the radial coordinate. For the height of the QD, we use $h_{QD}=8$ nm and for the base diameter, we use $d_{QD}=30$ nm (at height $0.1h_{QD}$). We assume the QDs to be located on a thin InAs layer ($h_{WL}=0.283$ nm) resembling the wetting layer (WL).

III. GALLIUM AND INDIUM INTERDIFFUSION DUE TO ANNEALING

Postgrowth thermal annealing of a heterostructure with self-assembled InAs/GaAs quantum dots leads to indium and gallium interdiffusion between dots and barriers.[8,9,14,15] Like other authors,[15] we consider this process in a continuum model because the diffusion length scales are much larger than the lattice constant. Besides we assume the diffusion coefficient to be independent of space coordinates so that we can describe the diffusion by Fick's law,

$$\frac{\partial x(\boldsymbol{r},t)}{\partial t} - D\Delta x(\boldsymbol{r},t) = 0, \tag{1}$$

where $x(\boldsymbol{r},t)$ is the position-dependent indium fraction in the $In_xGa_{1-x}As$ solid solution of the QD, which has been annealed for a time t and D is the diffusion constant. For solving the diffusion equation, initial conditions have to be set for $x(\boldsymbol{r},t)$. Here we assume that the as-grown QD is pure InAs so that the initial conditions are,

$$x(\boldsymbol{r},0) = \begin{cases} 1, & \text{inside QD/WL} \\ 0, & \text{inside the barrier layers.} \end{cases} \tag{2}$$

Fick's equation is solved by an ansatz, with separated cylindrical coordinates, without explicit dependence on the azimuthal angle due to the cylindrical symmetry, which is preserved during annealing.

For numerical treatment, we choose the computation region to be a cylinder with height $H_{Cyl}=80$ nm and diameter $D_{Cyl}=80$ nm. These values are much larger than the diffusion length of indium atoms in InAs/GaAs semiconductors (<10 nm for annealing temperatures up to 1000 °C). This fixing has to be supplemented with appropriate boundary conditions. The Dirichlet boundary conditions, $\chi=0$, are imposed on boundaries 1 and 3 because they are far from the QD (see Fig. 2). We also assume that the indium flux through boundary 2 is zero because in its neighborhood, the In atoms diffuse from the WL along the perpendicular direction as evident from the local symmetry of the problem. This can be included by the Neumann boundary condition $\boldsymbol{n}\cdot\vec{\nabla}\chi=0$, where $\boldsymbol{n}$ is the normal vector to the boundary directed outward. Also on boundary 4, the Neumann boundary conditions must be imposed for nulling the diffusion flux across the QD symmetry axis.

Using a finite element technique, we solve the diffusion problem with different diffusion constants for a fixed annealing time $t=30$ sec. We assume the Arrhenius equation for the temperature dependence of the diffusion constant,

$$D(T_a) = D_0 \exp\left[-\frac{E_A}{kT_a}\right], \tag{3}$$

where T_a is the annealing temperature, E_A is the activation energy of the interdiffusion process, and D_0 is a constant. E_A and D_0 are fitting parameters, whose values were optimized to get the best agreement between the measured and calculated PL transition energies of the annealed QDs (see Sec. IV and Appendix 3). We found $E_A=1.23$ eV and $D_0=8.5\times10^{-14}$ m^2/s. The obtained value of E_A is approximately three times smaller than the reported value in Ref. 14 for annealed InGaAs QDs. The diffusion length $L_D=\sqrt{[Dt]}$ is also larger in our calculations ($L_D=3.6$ nm vs $L_D\simeq1.5$ nm in Ref. 9 at 900 °C). The origin of this discrepancy is unclear. Variations of the parameters in our QD model (size, band offset, and strain energy, see Sec. IV and Appendix 3) over ranges where the calculations agree to experiment (see Sec. IV and Appendix 3) do not change the activation energy notably.

Figure 3 shows examples of the In distribution over the heterostructure calculated for the as-grown QDs [Fig. 3(a)] and QDs annealed at different temperatures [Figs. 3(b)–3(d)]. The annealing of the heterostructure leads to a rapid dissolution of the InAs QD into the GaAs barrier layers. The average indium content does not exceed 25% for QDs annealed at temperatures above 980 °C. In addition, the QD volume increases with annealing temperature.

IV. GROUND-STATE TRANSITIONS OF ANNEALED QUANTUM DOTS

For addressing the hyperfine interaction, we formally need only the distribution of nuclei and also the distribution of the electron wave function in the dot. In order to obtain a realistic modeling, we went one step further and calculated the energy of the ground-state transition in dependence of the annealing temperature and compared it to experimental photoluminescence data. Since the focus is not on obtaining a detailed description of the band structure, we have used a

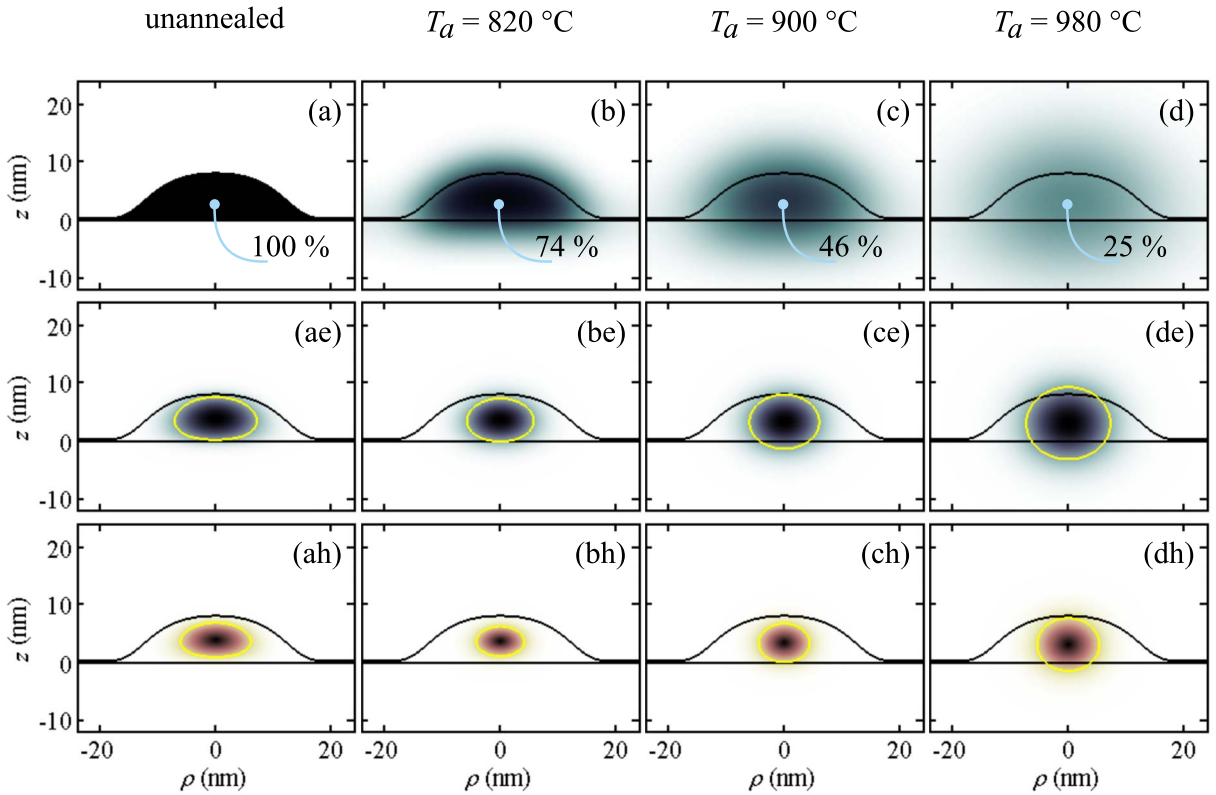

FIG. 3. (Color online) (a)–(d) Cross sections of calculated distributions of the indium content x over the heterostructure (as grown and thermally annealed at different temperatures). Highest values of indium concentration are marked in percents for each QD. Thin black line shows the as-grown QD shape. (ae)–(de) Distributions of the ground-state electron density in the as-grown and annealed QDs. Cuts through the probability density isosurface at the 33% level of the maximum density $|\psi|^2_{\max}$ are shown by the thin yellow ellipse in each panel. (ah)–(dh) Distributions of the ground-state hole densities, in analogy to the mid panels.

rather simple model for this purpose. A detailed description of this model is given in the Appendix, we give only a brief summary here. We have calculated the electron and hole states by solving the single-particle Schrödinger equation in effective-mass approximation. The confinement is created by the position-dependent difference of the band-gap energies between the GaAs barrier and the QD material. The potentials in the Schrödinger equation are obtained by distributing this difference between conduction and valence band and also including strain effects. Potential profiles obtained in such a way are shown in Fig. 4 for different annealing temperatures. Also the resulting energies of the electron and hole ground states are shown there and the corresponding probability densities are presented in the mid panels (ae)–(de) of Fig. 3 for the electrons and in the lower panels (ah)–(dh) of the same figure for the holes.

At low annealing temperatures (less than 820 °C), the QD shape is changed so little that it almost does not affect the carrier distributions. The changes of the potential even promote some additional localization of the carriers. Annealing at higher temperatures leads to an increase in the carrier localization volume and more spherical carrier density distributions, reflecting the increased sphericity of the indium concentration. As a consequence of these changes, the QD annealing leads to a decrease in the potential-well depth and

TABLE I. Nuclear parameters taken from Refs. 29 and 40.

Nuclei	In	Ga[a]	As
Nuclear spin I	9/2	3/2	3/2
Hyperfine constant $A(\mu\text{eV})$	56	42	46

[a]Average between ^{69}Ga and ^{71}Ga.

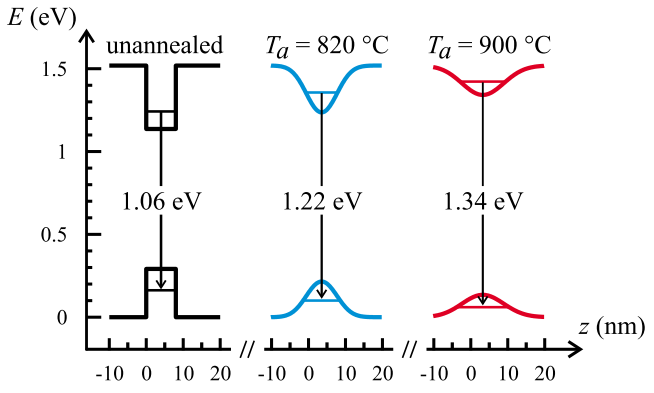

FIG. 4. (Color online) Potential profiles for the valence and conduction bands along the symmetry axis (ρ=0) of as-grown QDs and QDs annealed at different temperatures. The energies of the lowest electron and hole states are shown by thin horizontal lines in each well. The calculated energies of the ground optical transitions are shown in eV.

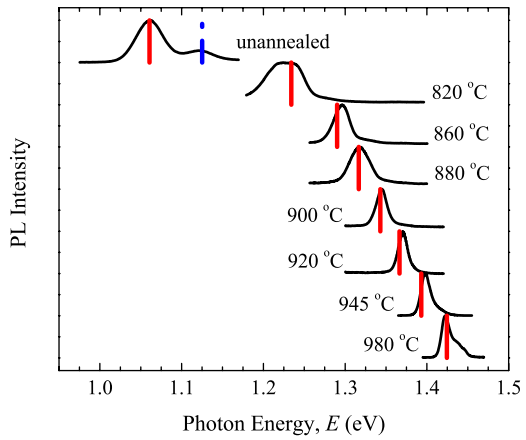

FIG. 5. (Color online) Calculated energies of the lowest optical transitions (solid vertical lines) in comparison with the PL spectra for the as-grown QDs and QDs annealed at different temperatures. The dashed-dotted line shows the energy position of the optical transition between the first-excited electron and hole states in the as-grown QDs.

also of the energy separation between the energy levels and the bottom of the potential well (see Fig. 4). The energies of the optical transitions, however, increase in the annealed QDs. From the electron and hole ground states, the energies of the transition between them was calculated, for which the Coulomb attraction was also included perturbatively.

The parameters in the model and the diameter and height of the as-grown QDs, as well as the strain energies, were adjusted such that agreement was achieved between theory and experiment for the whole series of annealed samples. This comparison for the as-grown QDs and the QD samples that are annealed at different temperatures is shown in Fig. 5, where the vertical lines give the calculated transition energies, while the traces give photoluminescence spectra recorded on the corresponding samples. These spectra were recorded using laser excitation with photon energy $E_{ex}=2.54$ eV at a temperature $T=1.6$ K.

The dependence of the energy of the ground-state transition $0e \rightarrow 0h$ on annealing temperature is well described by the calculations, confirming that the modeling of the QD annealing by the diffusion model gives reasonable results. The higher lying PL peaks that are seen for some samples correspond to recombination from the first-excited electron and hole states, $1e \rightarrow 1h$, as confirmed by high-excitation PL experiments in magnetic fields up to 28 T (not shown here), which to lowest approximation, can be described by a Fock-Darwin spectrum.[28]

V. HYPERFINE INTERACTION OF THE LOCALIZED ELECTRON WITH NUCLEI

A. Nuclear spin fluctuations in InGaAs quantum dots

As discussed in the Introduction, the electron-spin polarization is efficiently destroyed in a QD ensemble by the hyperfine interaction with randomly oriented nuclear spins, as reported in Ref. 4. The interaction of the electron and nuclear spins is described by a Fermi-type contact interaction,[4]

$$\hat{\mathcal{H}}_{hf} = v_0 \sum_j A_j (\hat{\mathrm{S}} \cdot \hat{\mathrm{I}}_j) |\psi(\boldsymbol{R}_j)|^2, \tag{4}$$

where $\hat{\mathbf{S}}$ and $\hat{\mathbf{I}}_j$ are the electron spin and the jth nucleus spin, respectively, $A_j = [16\pi\mu_B\mu_j/(3I_j)] \cdot |u_c(\boldsymbol{R}_j)|^2$ is the hyperfine coupling constant of the electron with the jth nucleus, μ_B is the Bohr magneton, and v_0 is the unit-cell volume. I_j, μ_j, and $\boldsymbol{R}_j$ are spin magnitude, magnetic moment, and position of the jth nucleus, respectively. $\psi(\boldsymbol{R}_j)$ and $u_c(\boldsymbol{R}_j)$ are the electron envelope and Bloch wave function at the nuclear site, respectively.

Due to the limited number of nuclei in a QD, which interact with the electron spin, a random orientation of the nuclear spins gives nonzero total spin with a magnitude fluctuating from dot to dot. The total nuclear spin acts on the electron spin as an effective hyperfine magnetic field $\boldsymbol{B}_N$. We consider nonpolarized and noninteracting nuclear spins, since magnitude and orientation of the effective field are random and can be described by a normal distribution,[4]

$$w_B = \frac{1}{(\sqrt{2\pi}\Delta_B)^3} \exp\left[-\frac{(\boldsymbol{B}_N)^2}{2\Delta_B^2} \right]. \tag{5}$$

Unlike in the paper by Merkulov *et al.*,[4] we define the variance of the effective magnetic field Δ_B, such that it approximately corresponds to the half width at half maximum of the normal distribution (5).

The effective magnetic field depends on both the hyperfine interaction energy and the electron g factor. Therefore, we write the variance Δ_B in the form $\Delta_B = \Delta_E/(\mu_B g_e)$, where g_e is the electron g factor, μ_B is the Bohr magneton, and Δ_E is the variance of the energy of the hyperfine interaction with the nuclear-spin fluctuations. The energy variance is determined similar to Ref. 4,

$$\Delta_E^2 = \frac{v_0^2}{3} \sum_j I_j(I_j+1) A_j^2 |\psi(\boldsymbol{R}_j)|^4. \tag{6}$$

There are three types of nuclei in InGaAs QDs. We consider the fluctuating nuclear field as a sum of three independent contributions with a normal distribution for each of them. Therefore, the squared total energy variance has to be calculated as sum of the squared energy variances of the different individual contributions,

$$\Delta_E^2 = (\Delta_E^{\mathrm{In}})^2 + (\Delta_E^{\mathrm{Ga}})^2 + (\Delta_E^{\mathrm{As}})^2, \tag{7}$$

where the Δ_E^{In}, Δ_E^{Ga}, and Δ_E^{As} are the contributions of each type of nuclei,

$$(\Delta_E^{\xi})^2 = \frac{v_0^2}{3} \sum_{j_\xi} I_{j_\xi}(I_{j_\xi}+1) A_{j_\xi}^2 |\psi(\boldsymbol{R}_{j_\xi})|^4, \tag{8}$$

with

$$\xi = \mathrm{In}, \mathrm{Ga}, \mathrm{As}.$$

Here the sum goes only over all nuclei of the same type. Supposing that the electron envelope wave function is constant over the crystal unit cell and replacing the sum over unit cells by an integration over the heterostructure volume, we obtain

$$(\Delta_E^{\mathrm{In}})^2 = C_{\mathrm{In}} \int |\psi(\boldsymbol{r})|^4 x(\boldsymbol{r}) d^3 r,$$

$$(\Delta_E^{\mathrm{Ga}})^2 = C_{\mathrm{Ga}} \int |\psi(\boldsymbol{r})|^4 [1 - x(\boldsymbol{r})] d^3 r,$$

$$(\Delta_E^{\mathrm{As}})^2 = C_{\mathrm{As}} \int |\psi(\boldsymbol{r})|^4 d^3 r, \tag{9}$$

with the indium fraction $x(\boldsymbol{r})$, which determines the probability to find an indium nucleus at the position $\boldsymbol{r}$. The constants C_ξ are given by

$$C_\xi = \frac{v_0}{3} I_\xi (I_\xi + 1) A_\xi^2, \quad \xi = \mathrm{In}, \mathrm{Ga}, \mathrm{As}. \tag{10}$$

Next, we introduce a new parameter, the effective average indium fraction in the QD,

$$\mathbf{x}_{\mathrm{eff}} = \frac{\int |\psi(\boldsymbol{r})|^4 x(\boldsymbol{r}) d^3 r}{\int |\psi(\boldsymbol{r})|^4 d^3 r}. \tag{11}$$

Using the electron localization volume defined in Ref. 4,

$$V_L = \left[\int |\psi(\boldsymbol{r})|^4 d^3 r \right]^{-1} \tag{12}$$

we come to the final expression for the total-energy variance,

$$\Delta_E^2 = \frac{1}{V_L} [C_{\mathrm{In}} \mathbf{x}_{\mathrm{eff}} + C_{\mathrm{Ga}} (1 - \mathbf{x}_{\mathrm{eff}}) + C_{\mathrm{As}}]. \tag{13}$$

We have calculated the effective indium fraction and the electron localization volume as a function of the QD annealing temperature [Fig. 6(a)]. Then, using Eq. (13), we have determined the total-energy variance and the partial contributions of each type of nuclei [Fig. 6(b)]. In these calculations, we used nuclear parameters collected in Table I.

As seen from Fig. 6(a), the electron localization volume increases and the effective indium fraction decreases with annealing temperature. These tendencies result in a decrease in the energy variance and, correspondingly, in the hyperfine interaction of the electron with the unpolarized nuclei due to the following physical reasons: Increase in V_L caused by: (i) a decrease in the contribution of each nucleus to the hyperfine interaction because of the reduction of the electron density at the nucleus and (ii) an averaging of the contributions over an increasing number of nuclei. Decrease in $\mathbf{x}_{\mathrm{eff}}$ causes by (iii) decrease in the contribution of the In nuclei, which have the largest angular momentum ($I_{\mathrm{In}}=9/2$). As seen from the figure, the In contribution, however, dominates up to the highest annealing temperatures, in spite of the considerable reduction of the In fraction in the QDs.

B. Suppression of the nuclear-spin fluctuations by the external magnetic field

The electron-spin relaxation caused by the nuclear fluctuation field can be suppressed by applying an external magnetic field.[4] In the presence of such an external magnetic field, the electron spin precesses about the total field, $\boldsymbol{B}_T = \boldsymbol{B}_{\mathrm{ext}} + \boldsymbol{B}_N$ (see inset in Fig. 7). For sufficiently large external fields, the nuclear-spin fluctuations almost do not contribute to the total field and, therefore, the electron-spin polarization does not decay.

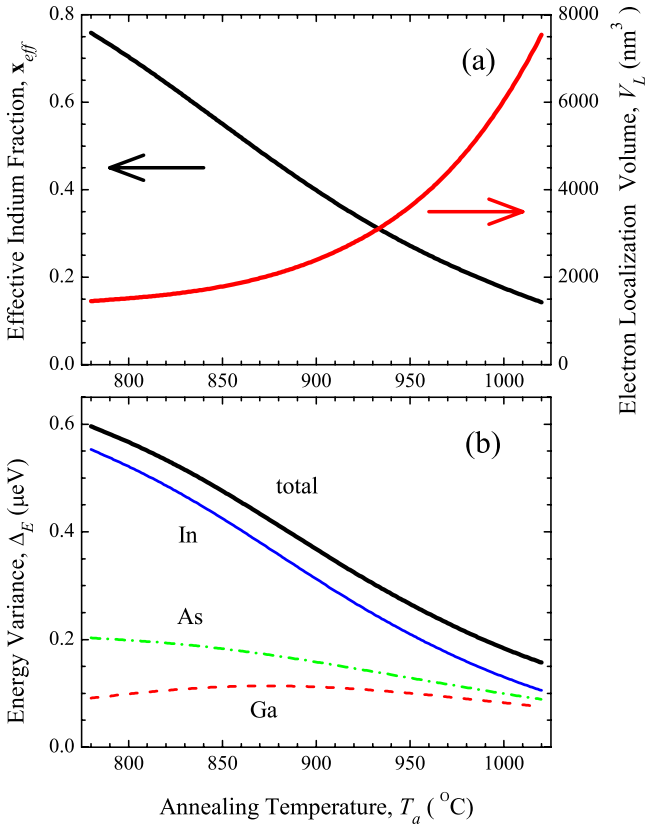

FIG. 6. (Color online) (a) Dependencies of the electron localization volume (red) and effective indium fraction in the QD (black) on annealing temperature. (b) The energy variance of hyperfine interaction of electron with nuclear-spin fluctuations and partial contributions of each type of nuclei as functions of annealing temperature.

Let us analyze this effect in more detail. We consider the projection of the electron spin (z projection) onto the axis of optical excitation. The direction of the external magnetic field (longitudinal field) coincides with the z axis (Faraday configuration). The spin z projection should be averaged over many periods of electron-spin precession about the total field and also over the QD ensemble. The time averaging allows us to calculate the constant component measured in such experiments. Although all the QDs in the ensemble are identical in our model, averaging over the ensemble occurs due to the random magnitude and orientation of the nuclear-spin fluctuations. The spin projection is calculated as

$$\langle S_z \rangle = \int \int \int_{-\infty}^{\infty} S_z(B_{\mathrm{ext}}) w_B(\boldsymbol{B}_N) d^3 B_N. \tag{14}$$

Here, the probability distribution $w_B(\boldsymbol{B}_N)$ is given by Eq. (5) and $S_z(B_{\mathrm{ext}})$ is given by

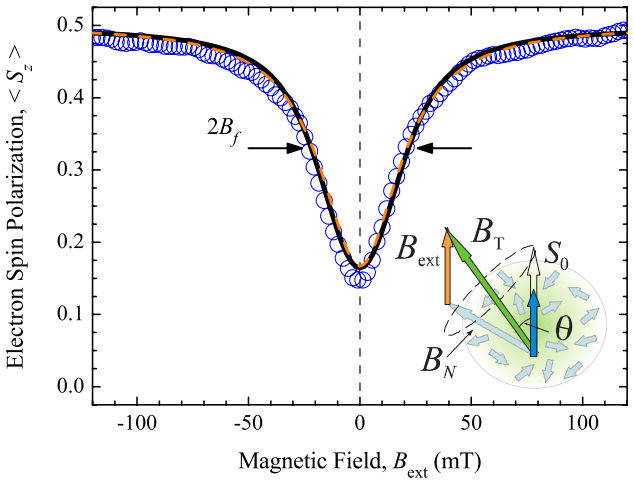

FIG. 7. (Color online) Calculated external magnetic-field dependence of the electron-spin polarization in the QDs that are annealed at T_a=900 °C (solid line) compared with the experiment (Ref. 35) (circles). The dashed line is obtained by approximating the calculations by a Lorentzian function [Eq. (18)]. Inset shows schematically the mechanism of suppression of nuclear-spin fluctuations by an external magnetic field.

$$S_z(B_{\text{ext}}) = S_0[\cos\ \theta(B_{\text{ext}})]^2 = S_0\frac{(B_{N_z}+B_{\text{ext}})^2}{(B_{N_z}+B_{\text{ext}})^2+B_{N_x^2}+B_{N_y^2}}, \tag{15}$$

where S_0 is the initial electron-spin polarization (we assume here $S_0=1/2$) and θ is the angle between the z axis and the total magnetic-field direction (see inset in Fig. 7). Note that Eq. (14) is the result of averaging over the ensemble of electron-spin projections and Eq. (15) is the result of time averaging of the electron-spin precession. The fast precession of the electron spin about B_T conserves only the projection of the initial spin S_0 on the direction of B_T so that $S=S_0\cos\theta$. Therefore, the measurable quantity is $S_z=S\cos\theta=S_0\cos^2\theta$.

The values of Δ_E that are found above [see Fig. 6(b)] allow us to calculate the dependence of $\langle S_z\rangle$ on the external magnetic-field strength for the annealed QDs using the relation $\Delta_B=\Delta_E/(g_e\mu_B)$ and the electron g factor values found experimentally.[30] Result of such calculations for QDs annealed at T_a=900 °C is shown in Fig. 7. We used $g_e=-0.6$ obtained from the linear interpolation between values $g_e=-0.65$ for $In_{0.6}Ga_{0.4}As$ QDs (Refs. 31–33) and $g_e=-0.54$ for the QDs annealed at T_a=945 °C (Ref. 34). The transverse g factor values were used here because only the x and y components of the fluctuating nuclear field depolarize the electron spin.

Dependence of $\langle S_z\rangle$ on B_{ext} has a dip around zero external field, which is due to the depolarization of the electron spin by the effective nuclear field. The electron-spin depolarization is not complete but one third of the initial polarization S_0 is retained. This result can be simply understood. We may decompose the arbitrarily oriented nuclear fields into three components oriented along the x, y, and z axes, each with equal probability/strength $P=1/3$. Then we may write the magnetic-field dependent z projection of the electron spin upon action of one of these components,

$$B_N \| x,y: \quad S_z = S_0\frac{B_{\text{ext}}^2}{B_{\text{ext}}^2+B_N^2},$$

$$B_N \| z: \quad S_z = S_0. \tag{16}$$

The nuclear fields along the x and y axes totally depolarize the electron spin at zero external magnetic field and the nuclear field along the z axis maintains its initial value. Supposing that the nuclear field components have identical average magnitude, which we express by $B_{N_{x,y,z}}\simeq 2\Delta_B$, the average electron-spin polarization can be written as

$$\bar{S}_z = S_0\left[\frac{1}{3}+\frac{2}{3}\frac{B_{\text{ext}}^2}{B_{\text{ext}}^2+(2\Delta_B)^2}\right]. \tag{17}$$

Rearrangement of the terms in this equation gives a magnetic-field dependence with a Lorentzian dip,

$$\bar{S}_z = S_0\left\{1-\frac{2/3}{1+[B_{\text{ext}}/(2\Delta_B)]^2}\right\}. \tag{18}$$

As seen from Fig. 7, the calculated field dependence of $\langle S_z\rangle$ can be well approximated by such a Lorentz function.

We can characterize the hyperfine interaction strength by the averaged nuclear field $B_f\simeq 2\Delta_B$, which we define as the half width at half minimum (HWHM) of the dip. This means that B_f and its dependence on the QD annealing temperature can be obtained from the magnitudes of the Δ_E shown in Fig. 6(b) using appropriate electron g factor values.

The electron-spin polarization in the QDs annealed at 900 °C was experimentally studied in the paper by Cherbunin, *et al.*[3] The authors have measured the circular PL polarization of singly negatively charged QDs and have found that the polarization is closely related to the spin orientation of the resident electron. The magnetic-field dependence of the PL polarization was found to reveal a dip around $B_{\text{ext}}=0$. One of the experimental curves measured at an excitation density 4.4 W/cm^2 is shown by circles in Fig. 7. As seen from comparison, the calculated and experimental curves are very similar. The calculated HWHM value $B_f^{(\text{th})}=22$ mT is close to the experimental one $B_f^{(\text{exp})}\simeq 24$ mT.

As it is found in the experiments reported in Ref. 3, quantity $B_f^{(\text{exp})}$ depends on the pump power density of excitation. We compare our calculations with the results measured at the relatively low excitation density when the nuclear-spin system is almost not disturbed. The value of $B_f^{(\text{exp})}$ that is estimated under extrapolation of the excitation density to zero is of about 30 mT. The value of $B_f^{(\text{th})}$ that we obtained is somewhat smaller, it indicates some overestimation of the QD volume in the unannealed heterostructure, which is probably due to oversimplified modeling of the QD energy structure. We consider the disagreement of quantities $B_f^{(\text{exp})}$ and $B_f^{(\text{th})}$ as relatively small by taking into account that no fitting parameters were used at modeling the hyperfine interaction of the resident electron with the nuclear-spin fluctuations.

VI. CONCLUSION

Theoretical modeling of InAs/GaAs QDs allowed us to simulate the effect of nuclear-spin fluctuations on the electron-spin polarization. First we determined the electron localization volume and the effective indium fraction in the QDs for different annealing temperatures. Due to interdiffusion of In and Ga during the annealing process, the QD size increases and, correspondingly, the electron localization volume considerably increases (from ~1700 nm^3 for as-grown QDs to ~4900 nm^3 for QDs annealed at 980 °C). At the same time, the dissolution of the QD results in a decrease in the effective indium concentration in the QDs. We calculated the partial contributions of the indium, gallium, and arsenic nuclei in the QD to the interaction energy of the electron with the nuclear-spin fluctuations and found that the hyperfine interaction is determined mainly by the indium contribution. The effect of the nuclear fluctuations decreases with increasing annealing temperature due to (i) the increasing number of nuclei interacting with the electron and (ii) the decreasing indium concentration. Finally, we modeled the suppression of the nuclear-spin fluctuation in a longitudinal magnetic field. The calculated dip of the electron-spin polarization is very similar to the one observed in the experiment as reported in Ref. 3.

ACKNOWLEDGMENTS

The authors thank R. V. Cherbunin, I. Ya. Gerlovin, A. A. Kiselev, G. G. Kozlov, and I. A. Yugova for fruitful discussions. This work has been supported in part by the Russian Ministry of Science and Education under Grant No. RNP.2.1.1.362, by Russian Foundation for Basic Research, and by the Deutsche Forschungsgemeinschaft under Grant No. BA 1549/12-2.

APPENDIX

The ground-state transition energies that are in dependence of the annealing temperature were calculated according to the model described in the following:

1. Confinement potentials and effective masses

The diffusion of indium from the QDs into the barriers leads to a modification of the valence and conduction-band profiles. Using the indium content $x(\boldsymbol{r})$ calculated for the annealed QDs as input, we model the three-dimensional profiles of the confinement potentials as well as effective carrier masses. For the band gap of $In_xGa_{1-x}As$, we use a linear interpolation between the InAs and GaAs gaps,

$$E_g(\boldsymbol{r}) = E_g^{\mathrm{InAs}} x(\boldsymbol{r}) + E_g^{\mathrm{GaAs}}[1 - x(\boldsymbol{r})], \tag{A1}$$

where $E_g^{\mathrm{InAs}}=0.415$ eV and $E_g^{\mathrm{GaAs}}=1.519$ eV are the band gaps for InAs and GaAs, respectively.[16] Further, we use $Q_e/Q_h=76/34$ for the band-offset ratio, based on the data for InAs/GaAs in Refs. 17 and 18. An important complication is the large mismatch between the InAs and GaAs lattice constants giving rise to large built-in strain, which affects the potential profiles considerably.[13,18–23]

We include the strain in our model in a simple way. First let us consider an as-grown QD. The average hydrostatic strain in InAs/GaAs QDs is 7–10%, as obtained by calculations using the continuum elasticity theory[18,21–23] and the valence force field Keating model[18–21] that leads to a decrease in the conduction-band well depth by 350–500 meV. Moreover, the strain changes weakly over the QD volume and, therefore, the constant potential approximation gives reasonable results.[24] Here we assume a strain-induced energy shift by $\delta V_v=450$ mev so that the electron confinement potential is 390 meV. The confinement potential in the valence band is more complex than in the conduction band.[18,19,21–23] Still, following Califano *et al.*,[24] we use a simple constant potential with a strain energy of $\delta V_v=90$ meV in the valence band, which corresponds to a hole confining potential of 175 meV. With these parameters, the experiments can be well described (see Appendix 3).

The annealing leads to a redistribution of the indium concentration and to the relaxation of the built-in strain. We assume that the strain energy depends linearly on indium concentration. With the calculated distribution $x(\boldsymbol{r})$, the band gap $E_g(\boldsymbol{r})$, the band-offset ratio Q_e/Q_h, and the linear strain dependence on $x(\boldsymbol{r})$, we determine the confinement potential profiles by

$$V_{e,h}(\boldsymbol{r}) = Q_{e,h}[E_g(\mathrm{GaAs}) - E_g(\boldsymbol{r})] - \delta V_{c,v} x(\boldsymbol{r}). \tag{A2}$$

Cross sections of some calculated potentials along the z-axis profiles for different annealing conditions were shown in Fig. 4.

The strain also changes the effective carrier masses compared to the unstrained ones, since the compressive stress acting on the dot material alters the curvature of the bulk bands. Here we use the electron effective masses $m_e^*(\mathrm{GaAs})=0.0665m_0$ in GaAs (Ref. 16) and $m_e^*(\mathrm{InAs})=0.04m_0$ in the strained InAs (Ref. 24), with the free-electron mass m_0. The hole effective masses are $m_h^*(\mathrm{GaAs})=0.3774m_0$ and $m_h^*(\mathrm{InAs})=0.341m_0$ (Ref. 24). For the annealed QDs, we use a linear interpolation of the effective masses as function of indium concentration,

$$m_{e,h}^*(\boldsymbol{r}) = m_{e,h}^*(\mathrm{InAs}) x(\boldsymbol{r}) + m_{e,h}^*(\mathrm{GaAs})[1 - x(\boldsymbol{r})]. \tag{A3}$$

2. Electron and hole energy states

To compute the electron and hole states in the annealed heterostructure, we solve the corresponding one-band Schrödinger equations in effective-mass approximation,[23,25]

$$-\frac{\hbar^2}{2}\nabla\left[\frac{1}{m^*(\boldsymbol{r})}\nabla\,\psi(\boldsymbol{r})\right] + V(\boldsymbol{r})\psi(\boldsymbol{r}) = E\psi(\boldsymbol{r}), \tag{A4}$$

where $V(\boldsymbol{r})$ and $m^*(\boldsymbol{r})$ are the position-dependent potentials and electron (hole) effective masses and $\psi(\boldsymbol{r})$ is the envelope wave function of a carrier with energy E.

For obtaining normalized solutions of this equation using cylindrical coordinates, the relevant boundary conditions have to be fixed. The azimuthal part of the solution is given by $\exp(in\varphi)$, where n is an integer corresponding to the carrier's angular momentum. Here we are only interested in

electron (hole) states confined in the QD. Therefore, we can impose the Dirichlet boundary conditions on boundaries 1–3, $\eta_n(z,\rho)=0$, to provide wave-function damping in the barriers (see Fig. 2). For boundary 4, there are two different types of conditions.[25] For nonzero angular momentum ($n \geq 1$), the Dirichlet boundary conditions must be imposed to avoid divergencies on the symmetry axis ($\rho=0$). For $n=0$, we employ Neumann boundary conditions $\boldsymbol{n}\cdot\vec{\nabla}\psi=0$ to ensure existence of $\vec{\nabla}\psi$, where $\boldsymbol{n}$ is the outward normal vector to the boundary. Using a finite element technique, we solve the eigenvalue problems for the electron and hole states in the QDs, which are as grown and annealed at different temperatures.

3. Optical transition energies

For calculating the optical transition energies, we have also taken into account the electron-hole Coulomb interaction. A rigorous solution of this problem is difficult. However, since the localizing potential for the QD carriers is stronger than the electron-hole interaction, we ignore the Coulomb correlations in the electron and hole motion and estimate the Coulomb interaction energy E_C for fixed electron and hole distributions,[13,22,26,27]

$$E_C^{km} = \frac{e^2}{4\pi\varepsilon_0\varepsilon}\int\int \frac{|\psi_e^k(\boldsymbol{r}_e)|^2|\psi_h^m(\boldsymbol{r}_h)|^2}{|\boldsymbol{r}_e-\boldsymbol{r}_h|}d^3r_e d^3r_h, \quad \text{(A5)}$$

where ε is the average dielectric constant in the annealed QD and $\psi_e^k(\boldsymbol{r}_e)$ and $\psi_h^m(\boldsymbol{r}_h)$ are the envelope wave functions of electron and hole in the kth and mth energy state, respectively. Calculations show that E_C^{00} is about 21 meV for as-grown QDs and it decreases to 15 meV for QDs annealed at 980 °C. This energy is slightly smaller when the carriers are in excited states. We note that the obtained values agree well with values calculated more accurately using the Hartree approximation (~20 meV) (Ref. 18). For the strongly annealed QDs, these values are only slightly smaller than the single-particle level splittings, underlining the approximative character of our calculations.

Then the optical transition energies are calculated by

$$E_{km} = E_e^k + E_h^m + E_g^x - E_C^{km}, \quad \text{(A6)}$$

where E_e^k and E_h^m are the electron and hole energies with respect to the $In_xGa_{1-x}As$ conduction-band bottom and valence-band top and E_g^x is the $In_xGa_{1-x}As$ band-gap energy at the QD center.

4. Comparison with experiment

For comparison with experiment, the optical transition energies between the electron and hole ground states and also between the first-excited states have been calculated. The energy of the lowest optical transition mainly depends on QD size. At the same time, the separation between the excited and lowest transitions is mainly determined by the height-diameter ratio and the shape of the QD. The strain energies for valence and conduction bands, which we used as fitting parameters, mainly influence the shift of the whole optical transition series, but affect the separation between the transition energies only weakly. This allows us to determine height and diameter of the QDs by comparing the calculated to the measured PL spectra for the as-grown sample. Then, the annealing was modeled as described above.

As discussed before, the dependence of the ground-state transition energy on annealing in the experiment is well described by the calculations. However, for the $1e \rightarrow 1h$ transition energy, good agreement between calculations and experiment is obtained only for the as-grown sample. For the annealed QDs, the calculated transition energies overestimate the observations by about 20 meV. This disagreement is probably related to oversimplifying the description of strain distribution in our model. For calculating the spin relaxation by hyperfine interaction, which is the focus of this paper, we are only interested in the relative change of the ground-state electron wave-function extension by the annealing. Therefore, this disagreement should not be too important for the conclusions.

*m.yu.petrov@gmail.com

[1] D. Gammon, Al. L. Efros, T. A. Kennedy, M. Rosen, D. S. Katzer, D. Park, S. W. Brown, V. L. Korenev, and I. A. Merkulov, Phys. Rev. Lett. **86**, 5176 (2001).
[2] P.-F. Braun, X. Marie, L. Lombez, B. Urbaszek, T. Amand, P. Renucci, V. K. Kalevich, K. V. Kavokin, O. Krebs, P. Voisin, and Y. Masumoto, Phys. Rev. Lett. **94**, 116601 (2005).
[3] R. V. Cherbunin, T. Auer, A. Greilich, I. V. Ignatiev, R. Oulton, M. Bayer, D. R. Yakovlev, G. G. Kozlov, D. Reuter, and A. D. Wieck (unpublished); Also available in arXiv:0805.3247 (unpublished).
[4] I. A. Merkulov, Al. L. Efros, and M. Rosen, Phys. Rev. B **65**, 205309 (2002).
[5] A. V. Khaetskii, D. Loss, and L. Glazman, Phys. Rev. Lett. **88**, 186802 (2002).
[6] A. V. Khaetskii and Yu. V. Nazarov, Phys. Rev. B **61**, 12639 (2000).
[7] M. Kroutvar, Y. Ducommun, D. Heiss, M. Bichler, D. Schuh, G. Abstreiter, and J. J. Finley, Nature (London) **432**, 81 (2004).
[8] R. Leon, S. Fafard, P. G. Piva, S. Ruvimov, and Z. Liliental-Weber, Phys. Rev. B **58**, R4262 (1998).
[9] S. Fafard and Nì. Allen, Appl. Phys. Lett. **75**, 2374 (1999).
[10] The annealing may also reduce the number of point defects and, thus, improve the structure quality (Ref. 9) that suppresses the defect related electron spin relaxation mechanism.
[11] A. Greilich, R. Oulton, E. A. Zhukov, I. A. Yugova, D. R. Yakovlev, M. Bayer, A. Shabaev, Al. L. Efros, I. A. Merkulov, V. Stavarache, D. Reuter, and A. Wieck, Phys. Rev. Lett. **96**, 227401 (2006).
[12] W. Langbein, P. Borri, U. Woggon, V. Stavarache, D. Reuter, and

A. D. Wieck, Phys. Rev. B **69**, 161301(R) (2004).
[13] For example, see D. Bimberg, M. Grundmann, and N. N. Ledentsov, *Quantum Dot Heterostructures* (Wiley, New York, 1999).
[14] S. Malik, C. Roberts, R. Murray, and M. Pate, Appl. Phys. Lett. **71**, 1987 (1997).
[15] O. Gunawan, H. S. Djie, and B. S. Ooi, Phys. Rev. B **71**, 205319 (2005).
[16] H. Landoldt and R. Börnstein, *Numerical Data and Functional Relationships in Science and Technology*, Landolt-Börnstein, New Series, Group III, Vol. 17, Pt. A (Springer, Berlin, 1987).
[17] C. G. Van de Walle, Phys. Rev. B **39**, 1871 (1989).
[18] O. Stier, M. Grundmann, and D. Bimberg, Phys. Rev. B **59**, 5688 (1999).
[19] M. A. Cusack, P. R. Briddon, and M. Jaros, Phys. Rev. B **54**, R2300 (1996).
[20] O. L. Lazarenkova, P. von Allmen, F. Oyafuso, S. Lee, and G. Klimeck, Appl. Phys. Lett. **85**, 4193 (2004).
[21] C. Pryor, Phys. Rev. B **57**, 7190 (1998).
[22] M. Grundmann, O. Stier, and D. Bimberg, Phys. Rev. B **52**, 11969 (1995).
[23] L. R. C. Fonseca, J. L. Jimenez, J. P. Leburton, and R. M. Martin, Phys. Rev. B **57**, 4017 (1998).
[24] M. Califano and P. Harrison, Phys. Rev. B **61**, 10959 (2000).
[25] R. V. N. Melnik and M. Willatzen, Nanotechnology **15**, 1 (2004).
[26] For example, see L. D. Landau and E. M. Lifshitz, *Quantum Mechanics: Nonrelativistic Theory*, Course of Theoretical Physics Vol. 3 (Pergamon, Oxford, 1975).
[27] E. Dekel, D. Gershoni, E. Ehrenfreund, J. M. Garcia, and P. M. Petroff, Phys. Rev. B **61**, 11009 (2000).
[28] S. Raymond, S. Studenikin, A. Sachrajda, Z. Wasilewski, S. J. Cheng, W. Sheng, P. Hawrylak, A. Babinski, M. Potemski, G. Ortner, and M. Bayer, Phys. Rev. Lett. **92**, 187402 (2004).
[29] P. F. Braun, B. Urbaszek, T. Amand, X. Marie, O. Krebs, B. Eble, A. Lemaitre, and P. Voisin, Phys. Rev. B **74**, 245306 (2006).
[30] The electron g factor in the InAs/GaAs QDs is determined by the spin-orbit interaction and can be, in principle, calculated if details of the QD conduction and valence band structure (including besides the heavy and light hole also the split-off band) is correctly modeled (see, e.g., papers by Kiselev *et al.* (Ref. 36) Kotlyar *et al.* (Ref. 37) and Pryor *et al.* (Ref. 38) for details). We have estimated the g factor based on a simplified model described in the paper by Ivchenko and Kiselev (Ref. 39) and using the parameters determined by our model for the annealed QDs. The calculated value, $g_e=-0.61$, for QDs annealed at 900 °C is close to that estimated from experiment.
[31] M. Bayer, O. Stern, A. Kuther, and A. Forchel, Phys. Rev. B **61**, 7273 (2000).
[32] M. Bayer, G. Ortner, O. Stern, A. Kuther, A. A. Gorbunov, A. Forchel, P. Hawrylak, S. Fafard, K. Hinzer, T. L. Reinecke, S. N. Walck, J. P. Reithmaier, F. Klopf, and F. Schäfer, Phys. Rev. B **65**, 195315 (2002).
[33] The 60% indium content approximately corresponds to that for the QDs annealed at $T_a=840$ °C [see Fig. 6(a)].
[34] I. A. Yugova, A. Greilich, E. A. Zhukov, D. R. Yakovlev, M. Bayer, D. Reuter, and A. D. Wieck, Phys. Rev. B **75**, 195325 (2007).
[35] The authors thank R. V. Cherbunin for contributing the original experimental data from Ref. 3.
[36] A. A. Kiselev, E. L. Ivchenko, and U. Rössler, Phys. Rev. B **58**, 16353 (1998).
[37] R. Kotlyar, T. L. Reinecke, M. Bayer, and A. Forchel, Phys. Rev. B **63**, 085310 (2001).
[38] C. E. Pryor and M. E. Flatté, Phys. Rev. Lett. **96**, 026804 (2006); **99**, 179901 (2007).
[39] E. L. Ivchenko and A. A. Kiselev, Fiz. Tekh. Poluprovodn. (S.-Peterburg) **26**, 1471 (1992) [Sov. Phys. Semicond. **26**, 827 (1992)].
[40] *Handbook of Chemistry and Physics*, edited by R. C. Weast (The Chemical Rubber Company, Cleveland, Ohio, 2001).